AGU PUBLICATIONS

Global Biogeochemical Cycles

RESEARCH ARTICLE
10.1002/2015GB005087

Key Points:
- A function to predict the rate-depth profile of particulate organic carbon
- Vertically resolved POC degradation rate is a function of the POC rain rate
- Predicts realistic global denitrification and POC burial rates

Supporting Information:
- Table S1 caption
- Table S1

Correspondence to:
K. Stolpovsky,
kstolpovsky@geomar.de

Citation:
Stolpovsky, K., A. W. Dale, and K. Wallmann (2015), Toward a parameterization of global-scale organic carbon mineralization kinetics in surface marine sediments, *Global Biogeochem. Cycles*, *29*, 812–829, doi:10.1002/2015GB005087.

Received 5 JAN 2015
Accepted 11 MAY 2015
Accepted article online 14 MAY 2015
Published online 15 JUN 2015
Corrected 18 FEB 2016

This article was corrected on 18 FEB 2016. See the end of the full text for details.

Toward a parameterization of global-scale organic carbon mineralization kinetics in surface marine sediments

K. Stolpovsky[1], A. W. Dale[1], and K. Wallmann[1]

[1]GEOMAR Helmholtz Centre for Ocean Research Kiel, Kiel, Germany

Abstract An empirical function is derived for predicting the rate-depth profile of particulate organic carbon (POC) degradation in surface marine sediments including the bioturbated layer. The rate takes the form of a power law analogous to the Middelburg function. The functional parameters were optimized by simulating measured benthic O_2 and NO_3^- fluxes at 185 stations worldwide using a diagenetic model. The novelty of this work rests with the finding that the vertically resolved POC degradation rate in the bioturbated zone can be determined using a simple function where the POC rain rate is the governing variable. Although imperfect, the model is able to fit 71% of paired O_2 and NO_3^- fluxes to within 50% of measured values. It further provides realistic geochemical concentration-depth profiles, NO_3^- penetration depths, and apparent first-order POC mineralization rate constants. The model performs less well on the continental shelf due to the high sediment heterogeneity there. When applied to globally resolved maps of rain rate, the model predicts a global denitrification rate of 182 ± 88 Tg yr^{-1} of N and a POC burial rate of 107 ± 52 Tg yr^{-1} of C with a mean carbon burial efficiency of 6.1%. These results are in very good agreement with published values. Our proposed function is conceptually simple, requires less parameterization than multi-G-type models, and is suitable for nonsteady state applications. It provides a basis for more accurately simulating benthic nutrient fluxes and carbonate dissolution rates in Earth system models.

1. Introduction

Around three quarters of primary production that is exported from the surface ocean is regenerated in the water column, with the remaining fraction available for benthic mineralization [*Sarmiento and Gruber*, 2006]. Sedimentary processing of organic matter is thus globally important for the nutrient balance of the ocean, particularly on long (kyr) time scales [*Van Cappellen*, 2003]. Benthic mineralization rates tend to attenuate rapidly below the uppermost centimeters where the largest fraction of organic matter is respired [*Boudreau and Ruddick*, 1991; *Hedges et al.*, 1999; *Martin and Sayles*, 2004]. Consequently, the depth distribution of reactive organic matter strongly determines the flux of redox-sensitive elements across the sediment surface. Yet, broad trends in the attenuation of carbon oxidation in bioturbated surface sediments are unknown at the global scale. This presents a major challenge and source of uncertainty for an emerging generation of Earth system models (ESM) that are able to explicitly account for vertical redox structure of sediments [*Arndt et al.*, 2013].

Quantifying the rate of particulate organic carbon (POC) mineralization with depth in sediment models is usually achieved by specifying the reactivity a priori [*Berner*, 1980]. The simplest approaches consider one or more reactive fractions, each defined by an individual rate constant (so-called "G" models [*Jørgensen*, 1978]). At least three discrete fractions are required to accurately capture POC mineralization in surface sediments where highly labile fractions are concentrated [e.g., *Soetaert et al.*, 1996]. Although empirical relations have been proposed to describe first-order rate constants for POC mineralization at the global scale, they do not adequately capture the full reactivity spectrum of natural organic matter [*Müller and Mangini*, 1980; *Toth and Lerman*, 1977; *Tromp et al.*, 1995]. By contrast, continuum approaches treat organic matter as a continuous reactivity distribution [*Middelburg*, 1989; *Boudreau and Ruddick*, 1991]. They have the advantage over multi-G models in that they generally require fewer parameters to describe a greater range of degradation time scales. However, the rate constant in these approaches has time dependence, and in contrast to multi-G models, their application to the bioturbated zone is not easily achieved since particles of different ages are well mixed. The lack of a generalized approach

comprises the transferability of different models on the regional and global scales [*Arndt et al*., 2013]. Thus, there is a real need to derive simple mathematical descriptions of benthic mineralization that can be applied to bioturbated sediments and improve predictions of sediment feedbacks on ocean biogeochemistry and climate.

In this study we present a new kinetic model for describing the rate of POC degradation with depth in bioturbated marine sediments. It is empirically grounded and treats POC reactivity as a continuum rather than a set of discrete fractions. The novelty of our approach rests with the fact that the rate-depth profile of POC degradation, not the rate constant, is prescribed a priori. Furthermore, we show that it can be defined from the rain rate of POC to the sediment and is thus designed with global model applications in mind. We propose that this new model will more accurately describe the coupling between benthic and pelagic biogeochemistry in ESMs.

2. Database

Benthic fluxes of oxygen (O_2) and nitrate (NO_3^-) from sites distributed worldwide were taken from the database assembled by *Bohlen et al*. [2012]. Only in situ measurements from benthic chambers were assembled for water depths <1000 m because enhanced solute transport by irrigating animals is not captured accurately using ex situ core incubations or diffusive flux calculations from pore water concentration profiles [*Glud*, 2008; *Devol and Christensen*, 1993]. For depths >1000 m, bioirrigation is essentially zero and diffusive fluxes determined ex situ were also considered [*Glud*, 2008]. The database was expanded with new data from the Oregon/California margin [*Berelson et al*., 2013], the NW African margin [*Dale et al*., 2014], and the NW Iberian margin [*Alonso-Pérez and Castro*, 2014], giving a total of 185 paired O_2 and NO_3^- flux measurements (Table S1 in the supporting information). Eighty-two stations are on the continental shelf (0 to 200 m), 50 stations on the slope (>200 to 2000 m), and 53 lie in deeper waters (>2000 to 5100 m). The database includes sites from a broad range of settings encountered in the contemporary ocean, such as sediments underlying oxygen-deficient zones and sandy shelf environments. We also assembled ammonium (NH_4^+) fluxes from 135 sites which are used to calculate benthic carbon oxidation rates (see below). In what follows, NO_3^- fluxes are reported as the sum of $NO_3^- + NO_2^-$ and negative fluxes denote uptake by the sediment. Details on the ranges of O_2, NO_3^-, and NH_4^+ fluxes in the database are provided by *Bohlen et al*. [2012].

3. Numerical Model

3.1. Model Architecture

Benthic fluxes at each site were simulated using a 1-D reaction-transport model. The model considers a limited diagenetic network based on one solid species (POC) and five solutes in the uppermost 50 cm of sediment. Solutes considered were O_2, NO_3^-, nitrite (NO_2^-), NH_4^+, and so-called oxygen-demanded units (ODUs). The latter lumps together reduced products of anaerobic organic matter diagenesis such as sulfide, dissolved Fe(II) and Mn(II) [*Soetaert et al*., 1996]. The involvement of more variables is not warranted due to the higher number of parameterizations required yet poorly known at the global scale. POC was transported in the sediment by accumulation (burial) considering compaction and mixing by bioturbation. Solutes were transported by advection due to accumulation, molecular diffusion, and nonlocal transport by bioirrigation. Solute mixing by bioturbation is minor compared to molecular diffusion and was neglected. Partial differential equations were used to solve the concentration changes with time. For POC (in dry weight percent, %)

$$(1-\phi(x))\frac{\partial \mathrm{POC}(x)}{\partial t} = \frac{\partial\left((1-\phi(x))\cdot D_B(x)\frac{\partial \mathrm{POC}(x)}{\partial x}\right)}{\partial x} - \frac{\partial((1-\phi(x))\cdot v_{\mathrm{solid}}(x)\cdot \mathrm{POC}(x))}{\partial x} - \frac{\mathrm{RPOC}(x)}{\rho}\cdot\frac{\mathrm{AWC}}{1000}\cdot 100\% \quad (1)$$

where t (year) is time, x (cm) is depth below the sediment-water interface, ϕ (dimensionless) is porosity, D_B ($cm^2\,yr^{-1}$) is the bioturbation coefficient, v_{solid} ($cm\,yr^{-1}$) is the solid burial velocity, RPOC is the rate of POC degradation ($mmol\,cm^{-3}\,yr^{-1}$ of bulk sediment), *AWC* (12 g mol^{-1}) is the carbon atomic weight, ρ (2.5 g cm^3) is the dry sediment density and 1000 ($mmol\,mol^{-1}$) is a unit conversion factor.

For solutes ($C_i(x)$ in mmol cm^{-3} of pore fluid)

$$\phi(x)\frac{\partial C_i(x)}{\partial t} = \frac{\partial\left(\phi(x)D_S(x)\frac{\partial C_i(x)}{\partial x}\right)}{\partial x} - \frac{\partial(\phi(x)v_{\text{solutes}}(x)C_i(x))}{\partial x} + \phi(x)\alpha_i(C_i(0) - C_i(x)) + \Sigma\phi(x)\mathrm{R}_i(x) \quad (2)$$

where D_S (cm^2 yr^{-1}) is the tortuosity-corrected molecular diffusion coefficient of species i, α_i (year^{-1}) is the bioirrigation coefficient, and ΣR_i is the sum of biogeochemical reactions affecting C_i.

Sediment porosity was assumed to decline exponentially with sediment depth [*Boudreau and Bennett*, 1999]:

$$\phi(x) = \phi(f) + (\phi(0) - \phi(f)) \cdot \exp(-p_x \cdot x) \quad (3)$$

where $\phi(0)$ is porosity at the sediment-water interface, $\phi(f)$ is the porosity in compacted sediment, and p_x (cm^{-1}) is the attenuation coefficient.

Molecular diffusion coefficients were calculated from the coefficients in seawater (D_{SW}) at in situ salinity, temperature and pressure using the Stokes-Einstein equation, and further corrected for tortuosity according to the modified Weissberg equation [*Boudreau*, 1997]:

$$D_S(x) = \frac{D_{\text{SW}}}{1 - 2 \cdot \ln(\phi(x))} \quad (4)$$

Temperature and salinity were set to measured values where available and otherwise estimated with a salinity of 35 and temperature as given in the World Ocean Atlas 2009 [*Locarnini et al.*, 2010].

The burial velocities of solutes and solids in sediment undergoing steady state compaction were defined from the sediment accumulation rate, ω_{acc} (cm yr^{-1}) [*Berner*, 1980]:

$$v_{\text{solutes}}(x) = \frac{\phi(f) \cdot \omega_{\text{acc}}}{\phi(x)} \quad (5)$$

$$v_{\text{solid}}(x) = \frac{(1 - \phi(f)) \cdot \omega_{\text{acc}}}{1 - \phi(x)} \quad (6)$$

Bioturbation intensity decreased with depth in the sediment [*Christensen*, 1982]:

$$D_B(x) = D_B(0) \cdot \exp\frac{-x^2}{2x_S^2} \quad (7)$$

where $D_B(0)$ (cm^2 yr^{-1}) is the bioturbation coefficient at the sediment water interface and x_S (cm) is the halving depth.

Bioirrigation also decreased with sediment depth and was assumed to affect all dissolved species equally:

$$\alpha(x) = \alpha(0) \cdot \exp\left(\frac{-x}{x_{\text{irr}}}\right) \quad (8)$$

where $\alpha(0)$ (year^{-1}) is the irrigation coefficient at the sediment-water interface and x_{irr} (cm) is the irrigation attenuation coefficient.

The reaction network listed in Table 1 includes the major reactions of the O and N cycles. Mineralization of organic matter entailed aerobic respiration (R_1), nitrate reduction (R_2), nitrite reduction to N_2 (i.e., heterotrophic denitrification, R_3), and anaerobic respiration (R_4). The electron acceptors are used sequentially in the order O_2, NO_2^-, and NO_3^- using Michaelis-Menten kinetics [*Bohlen et al.*, 2011] and appropriate half-saturation constants (Table 2). Organic matter was chemically defined as $POC(NH_3)_{r\text{NC}}$ where rNC is the N:C molar ratio, such that POC mineralization releases N from organic molecules to the pore water in the form of NH_4^+ in this proportion. The stoichiometric coefficients relating POC oxidation to the reduction of electron acceptors (r_{O2}, r_{NO2}, and r_{NO3}) were defined assuming a carbon oxidation state of −0.45 instead of zero, i.e., more reduced than Redfield stoichiometry [*Anderson*, 1995; *Sarmiento and Gruber*, 2006]. Details on their calculation are provided elsewhere [*Dale et al.*, 2014]. NO_2^- dynamics are described explicitly to provide a more realistic coupling between heterotrophic denitrification, nitrification (R_5 and R_6), and anammox (R_7) [*Bohlen et al.*, 2011]. In this study, denitrification, that is, total fixed N loss as N_2, refers to the sum of N loss by R_3 and R_7.

Table 1. Reaction Network Used in the Model[a]

Process	Stoichiometry[b]	Rate Expression
R_1	$POC(NH_3)_{rNC} + r_{O2}\ O_2 \rightarrow \Sigma CO_2 + r_{NC}\ NH_4^+$	$\frac{RPOC}{\phi(x)} \cdot \frac{[O_2]}{[O_2]+K_{O_2}}$
R_2	$POC(NH_3)_{rNC} + r_{NO3}\ NO_3^- \rightarrow \Sigma CO_2 + r_{NC}\ NH_4^+ + r_{NO3}\ NO_2^-$	$\frac{RPOC}{\phi(x)} \cdot \frac{[NO_3^-]}{[NO_3^-]+K_{NO_3}} \cdot \frac{K_{NO_2}}{[NO_2^-]+K_{NO_2}} \cdot \frac{K_{O_2}}{[O_2]+K_{O_2}}$
R_3	$POC(NH_3)_{rNC} + r_{NO2}\ NO_2^- \rightarrow \Sigma CO_2 + r_{NC}\ NH_4^+ + \frac{1}{2}\ r_{NO2}\ N_2$	$\frac{RPOC}{\phi(x)} \cdot \frac{[NO_2^-]}{[NO_2^-]+K_{NO_2}} \cdot \frac{K_{O_2}}{[O_2]+K_{O_2}}$
R_4	$POC(NH_3)_{rNC}$ + "an oxidant" $\rightarrow \Sigma CO_2 + r_{NC}\ NH_4^+ + r_{O2}$ ODU	$\frac{RPOC}{\phi(x)} \cdot \frac{K_{NO_3}}{[NO_3^-]+K_{NO_3}} \cdot \frac{K_{NO_2}}{[NO_2^-]+K_{NO_2}} \cdot \frac{K_{O_2}}{[O_2]+K_{O_2}}$
R_5	$NH_4^+ + 1.5\ O_2 \rightarrow NO_2^- + H_2O + 2\ H^+$	$k_5 \cdot [O_2] \cdot [NH_4^+]$
R_6	$NO_2^- + 0.5\ O_2 \rightarrow NO_3^-$	$k_6 \cdot [O_2] \cdot [NO_2^-]$
R_7	$NH_4^+ + NO_2^- \rightarrow N_2 + 2\ H_2O$	$k_7 \cdot [NO_2^-] \cdot [NH_4^+]$
R_8	$ODU + O_2 \rightarrow$ an oxidant	$k_8 \cdot [O_2] \cdot [ODU]$
R_9	$ODU + 0.5\ NO_3^- \rightarrow$ an oxidant $+ 0.5\ NH_4^+$ for depths ≤ 200 m $ODU + 0.8\ NO_3^- \rightarrow$ an oxidant $+ 0.4\ N_2$ for depths > 200 m	$k_9 \cdot [NO_3^-] \cdot [ODU]$

[a]Model parameters are listed in Table 2. R_1 to R_4 correspond to carbon degradation, and the rates of production and consumption of other species follow the stoichiometry indicated.
[b]ΣCO_2 = dissolved inorganic carbon. Water is omitted from R_1 to R_4 for clarity.

Table 2. Model Parameters

Description	Value	Unit	Source
Temperature of the bottom water, T	Variable	°C	*Locarnini et al.* [2010]
Salinity of the bottom water, S	35	-	*Locarnini et al.* [2010]
Sediment accumulation rate, ω_{acc}	Variable[a]	$cm\ yr^{-1}$	*Burwicz et al.* [2011]
Bioturbation coefficient at surface, $D_B(0)$	Variable[b]	$cm^2\ yr^{-1}$	*Boudreau* [1997]
Bioturbation halving depth, z_{bt}	5	cm	*Boudreau* [1997] and *Teal et al.* [2008]
Bioirrigation coefficient at surface, $\alpha(0)$	Variable[c]	$year^{-1}$	*Meile and Van Cappellen* [2003]
Bioirrigation attenuation coefficient, x_{irr}	2	cm	*Archer et al.* [2002]
Porosity at sediment surface, $\varphi(0)$	Variable[d]	-	This study
Porosity in compacted sediment, $\varphi(f)$	$0.9 \cdot \varphi(0)$	-	This study
Porosity attenuation coefficient, p_x	0.2	cm^{-1}	This study
O_2:POC ratio for aerobic respiration, r_{O2}	118/106	mol O_2/mol C	*Dale et al.* [2014]
NO_3^-:POC ratio for nitrate reduction, r_{NO3}	236/106	mol NO_3^-/mol C	This study
NO_2^-:POC ratio for nitrite reduction, r_{NO2}	157.3/106	mol NO_2^-/mol C	This study
N:C ratio in organic matter, r_{NC}	16/106	mol N/mol C	*Redfield et al.* [1963]
Kinetic constant for NH_4^+ aerobic oxidation to NO_2^-, k_5	$0.15 \cdot 10^9$	$M^{-1}\ yr^{-1}$ of NH_4^+	[e]
Kinetic constant for NO_2^- aerobic oxidation to NO_3^-, k_6	$0.15 \cdot 10^9$	$M^{-1}\ yr^{-1}$ of NO_2^-	[e]
Kinetic constant for anammox, k_7	$0.30 \cdot 10^{10}$	$M^{-1}\ yr^{-1}$ of NO_2^-	[e]
Kinetic constant for aerobic ODU oxidation, k_8	$0.15 \cdot 10^9$	$M^{-1}\ yr^{-1}$ of ODU	[e]
Kinetic constant for anaerobic ODU oxidation, k_9	$0.15 \cdot 10^6$	$M^{-1}\ yr^{-1}$ of ODU	[e]
Michaelis-Menten constant for aerobic respiration, K_{O_2}	8	μM	[e]
Michaelis-Menten constant for nitrate reduction, K_{NO_3}	10	μM	[e]
Michaelis-Menten constant for nitrite reduction, K_{NO_2}	1	μM	[e]

[a]Calculated as a function of water depth.
[b]Calculated as a function of sediment accumulation rate: $D_B(0) = 15.7\ \omega_{acc}^{0.69}$.
[c]The average bioirrigation coefficient in surface sediments ($\overline{\alpha}$, $year^{-1}$) was calculated as a function of bottom water O_2 concentration and total sediment oxygen uptake [*Meile and Van Cappellen*, 2003]. Following *Thullner et al.* [2009], $\alpha(0)$ was calculated from $\overline{\alpha}$. The same irrigation coefficient was applied to all solutes, although this is only an approximation [*Meile et al.*, 2005].
[d]Surface porosity in fine-grained muds was taken to be 0.9 on the shelf and 0.95 in deeper waters [*Reimers et al.*, 1992; *Boudreau and Bennett*, 1999]. The model is not designed to simulate biogeochemical dynamics in sands since this requires a more complex description of pressure-driven advection rates through the surface sediments, which are poorly known at the global scale.
[e]Various sources, including *Van Cappellen and Wang* [1995], *Dhakar and Burdige* [1996], *Berg et al.* [2003], and *Bohlen et al.* [2011].

R_4 represents the sum of POC oxidation with "other oxidants" such as metal oxides and sulfate. The reaction product, ODU, can be oxidized by O_2 (R_8) or NO_3^- (R_9). We assumed that ODU mainly consists of sulfide in shelf sediments (<200 m water depths), such that NO_3^- is converted to NH_4^+ (e.g., during dissimilatory nitrate reduction to ammonium [*Otte et al.*, 1999]). On the slope and in deep-sea sediments, ODU consists mainly of dissolved reduced metals which can be oxidized by NO_3^- yielding N_2 [e.g., *Dhakar and Burdige*, 1996; *Hulth et al.*, 2005]. The diffusion coefficient for ODU is defined accordingly. By definition, oxidation of 1 mol of ODU requires four electrons, that is, 1 mol of O_2 or 0.8 mol of NO_3^- for reduction to N_2 or 0.5 mol of NO_3^- for reduction to NH_4^+ (Table 1).

3.2. Parameterization of Transport Process and Biogeochemical Reactions

The parameterization of transport processes relied on global empirical relationships where possible (Table 2). These relationships are essentially "best fit" empirical approximations using data from a range of different environments. They are associated with a high uncertainty due to the scatter caused by the natural heterogeneity of the seafloor and only approximate transport rates at any given location. Nonetheless, given the dearth of information on the distribution of transport rates in sediments at the global scale, there is currently no better alternative [*Archer et al.*, 2002]. Even less information is available about how the kinetic parameters in the model vary globally. Reported rate constants in diagenetic models for a given reaction often span many orders of magnitude [*Dale et al.*, 2012]. This is probably because they integrate the effect of several environmental variables, including ionic strength and pH, thermodynamic constraints, and microbial community structure. We parameterized the N cycle from a few selected studies where the constants were well constrained by field data (Table 2). It is nonetheless inevitable that some sites in the database will be inadequately represented by the broad approach adopted here. However, as shown later, those sites tend to adhere to specific types of environment for which our model is not designed to simulate.

3.3. POC Mineralization Kinetics

Continuum models are advantageous over multi-G models since they avoid the sometimes arbitrary partitioning of organic matter reactivity into a finite number of fractions each with a hard-to-define reactivity [*Middelburg*, 1989; *Boudreau and Ruddick*, 1991]. Continuum model theory assumes that the rate of POC degradation, RPOC(t), can be described as the sum of an infinite number of discrete fractions that are each degraded according to first-order kinetics [*Boudreau and Ruddick*, 1991]:

$$\mathrm{RPOC}(t) = \int_0^\infty k \cdot g(k,0) \cdot \exp(-k \cdot t)\mathrm{d}k \tag{9}$$

where $g(k,0)$ is a probability density function that determines the fraction of POC having a reactivity k at time $t = 0$ or more precisely the POC fraction having a reactivity between k and $k + \mathrm{d}k$ where $\mathrm{d}k$ is an infinitesimal increment in k. *Boudreau and Ruddick* [1991] proposed to assign the gamma distribution to $g(k,0)$, for which RPOC(t) can be expressed as

$$\mathrm{RPOC}(t) = \nu \cdot (a + t)^{-1} \cdot \mathrm{POC}(t) \tag{10}$$

where a (year) is defined as the average lifetime of the reactive components in the bulk POC pool and ν (dimensionless) controls the shape of the gamma distribution when $k \to 0$. In this case, $k(t)$ is equal to $\nu \cdot (a + t)^{-1}$. The power model proposed by *Middelburg* [1989] defines $k(t)$ analogously:

$$k(t) = h \cdot (\mathrm{age}_0 + t)^q \tag{11}$$

where age_0 denotes the apparent initial age of the organic matter mixture and h (0.16) and q (−0.95) are empirical constants derived from a database of apparent first-order rate constants [*Middelburg*, 1989]. The rate equations for the reactive continuum and power models are mathematically equivalent when $q = -1$.

These models show that the complete spectrum of POC reactivity can be described using a limited number of parameters compared to multi-G approaches, which require two parameters per fraction (reactivity and initial concentration). However, the age and reactivity of POC are poorly constrained in bioturbated surface sediments [*Middelburg*, 1989; *Boudreau and Ruddick*, 1991; *Meile and Van Cappellen*, 2005; *Rothman and Forney*, 2007]. Ages of reactive tracers within this layer depend on the burial velocity and bioturbation rate as well as the reactivity of the tracer [*Meile and Van Cappellen*, 2005]. So far, POC ages in bioturbated sediments have only been determined assuming simple first-order degradation kinetics

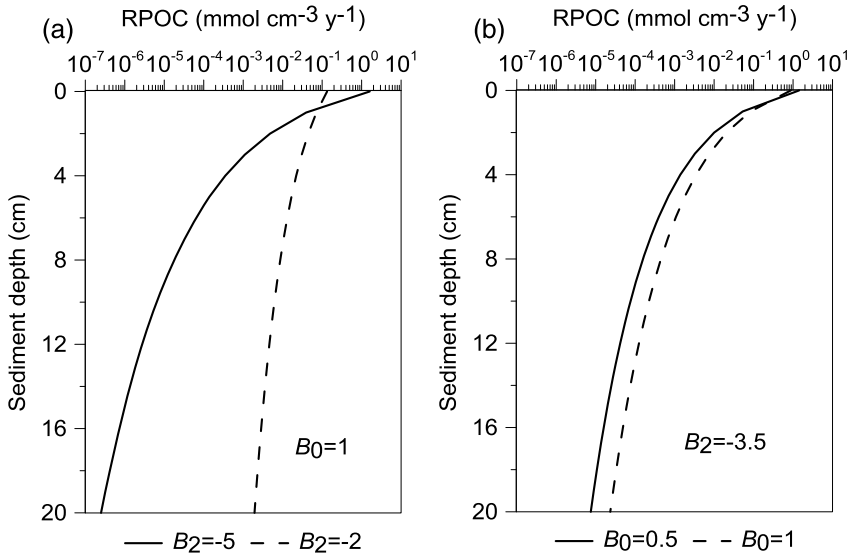

Figure 1. POC degradation rate as a function of (a) variable B_2 and fixed B_0 and (b) variable B_0 and fixed B_2. Note that the value of B_1 is calculated directly from B_2 for a given value of B_0 (equation (14)).

[*Meile and Van Cappellen*, 2005]. POC ages for the application of reactive continuum models are virtually unknown; a fact worsened by the fact that the more reactive POC fractions may be preferentially taken up and displaced by benthic macrofauna [*Smith et al.*, 1993].

For the present study, we assume that the rate of POC degradation in the bioturbated zone essentially follows the general form of the power law model. Replacing time, t, with depth, x, leads to the following function describing the depth-dependent rate of POC degradation (mmol cm^{-3} yr^{-1} of bulk sediment):

$$\mathrm{RPOC}(x) = B_0 \cdot (x + B_1)^{B_2} \tag{12}$$

where B_0 (mmol cm^{-3-B2} yr^{-1}), B_1 (cm), and B_2 (dimensionless) are parameters defining the shape of the decrease of the rate with sediment depth. The objective of this paper is to provide proof of concept for this approach by constraining the B coefficients with field data. We are aware that other functions defining a steep downcore decline in reactivity and reaction rate could also be used to fit the observations, and we strongly emphasize the purely empirical nature of the power function. We chose the power function rather than a different form because observations of POC degradation both in the laboratory and in marine sediments demonstrate that it provides a realistic description of time-dependent mineralization [*Middelburg*, 1989; *Boudreau and Ruddick*, 1991; *Boudreau et al.*, 2008].

If one assumes, as a first approximation, that the rain rate of POC to the seafloor (RRPOC, mmol cm^{-2} yr^{-1}) provides an upper limit of the total amount of POC available for degradation, then

$$\mathrm{RRPOC} = \int_0^\infty B_0 \cdot (B_1 + x)^{B_2} \mathrm{d}x \tag{13}$$

This purely theoretical approach implies that all POC will be degraded at infinite sediment depth. If RRPOC is known, the value of one parameter can be determined from the other two using equation (13). For example, for B_1

$$B_1 = \left(-(1 + B_2) \cdot \mathrm{RRPOC} \cdot B_0^{-1}\right)^{\frac{1}{1+B_2}} \tag{14}$$

This equation is valid for $B_2 < -1$. The effect of B_0 and B_2 on RPOC(x) is shown in Figure 1 for typical values derived in this study and a RRPOC of 10 mmol m^{-2} d^{-1}. Low B_2 values are associated with high rates of carbon degradation at the surface and a rapid decrease over the bioturbation layer by several orders of magnitude. By comparison, RPOC(x) is much less sensitive to variations in B_0, with lower values tending to shift the profile toward higher rates at the very surface and lower rates of degradation at greater sediment depth. Hence, the attenuation of RPOC(x) with sediment depth is mainly controlled by B_2, whereas B_0 exerts a relatively minor scaling effect over the range of 0.5 to 1 (see below).

RRPOC at each station was derived from the depth-integrated rate of POC degradation in the bioturbated layer, $RPOC_B$ (mmol cm^{-2} yr^{-1}), and the fraction of the POC deposited on the seafloor that is buried below the bioturbated layer:

$$RRPOC = \frac{RPOC_B}{100\% - CBE} \cdot 100\% \tag{15}$$

where CBE is the organic carbon burial efficiency in percent, calculated from the sediment mass accumulation rate (F_{sed}, g cm^{-2} yr^{-1}) using an empirical function [*Dale et al.*, 2012]:

$$CBE = \frac{A_1 - A_2}{1 + \frac{F_{sed}}{A_3}} + A_2 \tag{16}$$

$$F_{sed} = \rho_{sed} \cdot (1 - \phi_f) \cdot \omega_{acc} \tag{17}$$

where A_1 (0.5%), A_2 (75%), and A_3 (0.07 g cm^{-2} yr^{-1}) are parameters applicable to sediments underlying normal oxic bottom waters and ρ_{sed} is the density of dry sediment (2.5 g cm^{-3}). CBE is typically calculated at around 10 cm depth where POC content in surface sediments tends to reach asymptotic levels. This depth also broadly coincides with the average depth of the bioturbated layer [*Boudreau*, 1997; *Teal et al.*, 2008].

$RPOC_B$ was approximated from a mass balance of the measured benthic fluxes, J_i, where $i = O_2$, NO_3^-, and NH_4^+ [*Dale et al.*, 2014]:

$$RPOC_B = \frac{2 \cdot J_{NH4} \cdot \frac{472}{530} - J_{O2} \cdot \frac{472}{530} - J_{NH4} \cdot r_{O2} - J_{NO3} \cdot r_{O2}}{2 \cdot r_{NC} \cdot \frac{472}{530} - r_{NC} \cdot r_{O2} + \frac{472}{530} \cdot r_{O2}} \tag{18}$$

NH_4^+ fluxes were always directed out of the sediment and were negligible for sites >1000 m water depth [*Bohlen et al.*, 2012]. For shallower sediments where NH_4^+ flux data were unavailable, the median flux of the other stations was used instead. It should be noted that $RPOC_B$ calculated according to equation (18) includes a somewhat poorly defined contribution by degradation processes occurring in deeper sediment horizons underlying the bioturbated surface zone. A fraction of reduced solutes produced by oxidation of organic matter in deeper sediments will diffuse upward into the surface layers and be oxidized, thus contributing to the total sink of O_2 and NO_3^-. However, the fraction of reducing equivalents that are retained in sediments due to adsorption (e.g., NH_4^+ and Fe^{2+}) and mineral precipitation and burial (e.g., iron sulfides) as well as burial of dissolved solutes increases with sediment depth. Hence, although diagenesis is ongoing below the bioturbated layer, it will not be fully communicated to the oxidative sinks at the surface sediments. In addition, a fraction of the deposited POC is highly refractive (by nature of the power law) and does not undergo degradation on early diagenetic time scales. As an independent constraint on this approach, published rates of global POC burial are compared to the model-predicted values (see section 4.2.2).

3.4. Accuracy of Model Simulations

We used RRPOC as a governing parameter to find a relationship between B_2 and RRPOC that best determines the rate-depth profile of POC degradation together with the independent parameter B_0. The principle constraint on the POC degradation kinetics is the database of O_2 and NO_3^- fluxes. The simulated flux, $J_{c,i}$ where $i = O_2$ or NO_3^-, was considered to be acceptable if it was within a defined tolerance limit, Δ_i (mmol m^{-2} d^{-1}) of the measured flux:

$$J_{m,i} - \Delta_i < J_{c,i} < J_{m,i} + \Delta_i \tag{19}$$

Δ_i was defined as a fraction (d) of the measured flux, J_m, attributable to model error, and a minimum flux, γ (mmol m^{-2} d^{-1}):

$$\Delta_i = \left|J_{m,i}\right| \cdot d + \delta \qquad \text{where} \begin{cases} \delta = \gamma \ \ if \ \ \left|J_{m,i}\right| \cdot d < \gamma \\ \delta = 0 \ \ if \ \ \left|J_{m,i}\right| \cdot d \geq \gamma \end{cases} \tag{20}$$

d includes the uncertainty from various sources, such as the calculation of $RPOC_B$, CBE, and the global parameterizations. Considering these rather large uncertainties, modeled fluxes are shown against deviation intervals of $d = 25\%$ and 50% of $J_{m,i}$.

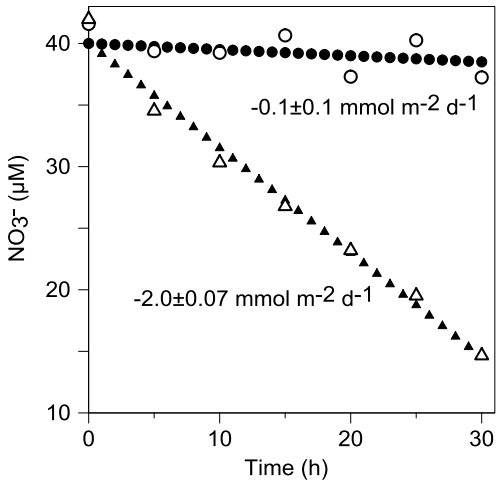

Figure 2. Hypothetical bottom water concentration time series for NO_3^- in a benthic incubation experiment. The solid circles and triangles denote an error-free decrease in NO_3^- corresponding to fluxes of 0.1 and 2.0 mmol m^{-2} d^{-1}, respectively, for an initial NO_3^- bottom water concentration of 40 µM. The open symbols denote the concentrations of seven subsamples withdrawn at discrete intervals from this time series to which a maximum ±5% random error has been added. The flux ± SE for each subsampled set of data is indicated.

It is necessary to define a minimum tolerance limit, γ, to provide some latitude for simulating the stations where measured fluxes are very low. This is because even very small absolute differences between the modeled and measured flux will translate into large relative errors as the fluxes get smaller. The γ was approximated as the lowest flux that is statistically larger than zero which can be estimated from a hypothetical sediment incubation experiment. To find this value, we first defined an error-free concentration time series for a 30 h sediment incubation experiment (Figure 2). We then selected seven of these points, at the start of the incubation and every 5 h thereafter, to which a maximum ±5% random error was added. This represents a typical subsampling frequency with errors due to natural heterogeneity, sample handling, analytical precision, and so on. The first example for NO_3^- (circles in Figure 2) shows that the flux calculated from the subsampled data is identical to the standard error (SE) when the absolute flux is 0.1 mmol m^{-2} d^{-1}; that is, the flux is indistinguishable from zero. As the flux increases, the relative SE decreases (triangles in Figure 2). It also decreases as the number of data points and the length of the incubation increase, an approach often needed to obtain reliable flux estimates in slowly accumulating sediments [e.g., *Jahnke and Jahnke*, 2004].

The minimum flux that can be calculated scales positively with bottom water concentration. For a typical bottom water O_2 concentration of 150 µM [*Thullner et al.*, 2009], the value of flux that is equal to the SE is 0.35 mmol m^{-2} d^{-1} for the subsampling frequency applied in Figure 2 (data not shown). Hence, we define these fluxes as the corresponding minimum tolerance limits (0.1 mmol m^{-2} d^{-1} for NO_3^- and 0.35 mmol m^{-2} d^{-1} for O_2). In other words, the modeled tolerance limit at sites where $|J_{m,i}|\, d < \gamma$ (i.e., very low measured fluxes) is set to these values. In practice, this applies to NO_3^- only, since almost all O_2 fluxes in the database are $>$ 0.35 mmol m^{-2} d^{-1}.

3.5. Boundary Conditions and Model Solution

Fixed concentrations were imposed for solutes (Dirichlet boundary) at the sediment surface ($x = 0$ cm). Measured bottom water concentrations were applied to O_2, NO_3^-, and NH_4^+, whereas NO_2^- and ODU were set to zero since they do not accumulate in seawater to a significant degree. The rain rate was used as a flux condition for POC. At the bottom ($x = 50$ cm), a zero gradient boundary was applied for all species (Neumann boundary). The set of coupled partial differential equations was solved using the NDSolve algorithm in MATHEMATICA 8 using finite differences [*Boudreau*, 1996] over an uneven grid with a total of 100 depth intervals. Close to the sediment-water interface where reaction rates are highest, a submillimeter-scale grid resolution was used, while at greater depth the resolution increased to a maximum of 1 cm. For each station, the model simulation time was sufficiently long (5 L/ω_{acc} years, where $L = 50$ cm) so that steady state was reached. The model was $>$99% mass conservative and a typical steady state run required $<$5 s on a personal computer (2.9GHz CPU and 8.0GB RAM).

4. Results and Discussion

4.1. Derivation of a Predictive Function for POC Mineralization in Sediments

Our objective was to find an empirical function relating the depth distribution of POC mineralization to rain rate (RRPOC). This is an attractive master variable because (i) POC fluxes to the seafloor are reasonably well known and routinely computed by ESMs [e.g., *Dunne et al.*, 2007] and (ii) POC reactivity appears to be

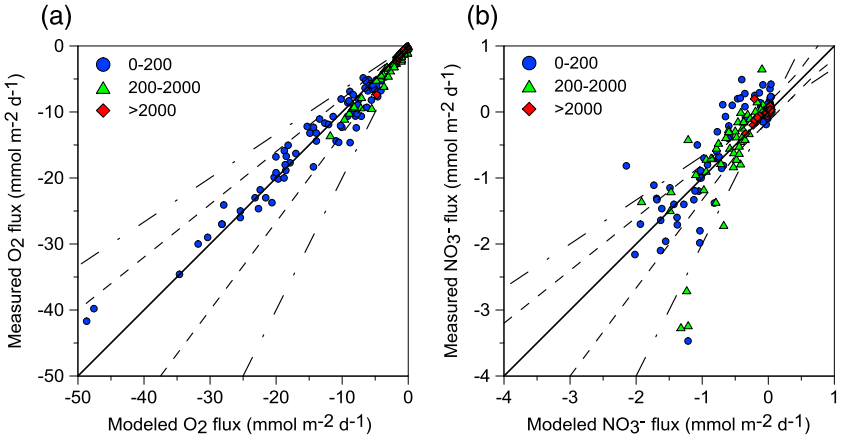

Figure 3. Measured versus modeled benthic fluxes of (a) O_2 and (b) NO_3^- using the optimized parameters of the transfer function (equation (21)) for shelf (0–200 m), slope (200–2000 m), and deeper sediments (>2000 m). The solid line indicates the 1:1 correlation (measured = modeled), the dashed lines indicate the 25% deviation, and the dash-dotted lines indicate the 50% deviation.

correlated with rain rate [*Emerson et al*., 1985; *Murray and Kuivila*, 1990; *Soetaert et al*., 1996; *Boudreau*, 1997; *Martin and Sayles*, 2006].

Due to the low sensitivity of RPOC(x) to B_0 (Figure 1), we began searching for the functional form of the relationship between B_2 and RRPOC that best simulated the entire database of O_2 and NO_3^- fluxes. Following many tests and sensitivity analyses, it became clear that B_2 was best described by a power law relationship of the type

$$B_2 = m \cdot \mathrm{RRPOC}^n \tag{21}$$

where m and n are empirical coefficients and RRPOC is in mmol m^{-2} d^{-1}. These coefficients were constrained by simulating the fluxes at all stations in the database collectively using a sorting algorithm. In this procedure we fixed the value of B_0 and m at their lowest values and varied the value of n with fixed step size (0.01). Subsequently, m was increased one step size (0.02), and the procedure was repeated after increasing the value of B_0 (step size 0.1) and so on over the complete range of parameters. The ranges of B_0, m, and n tested that gave realistic O_2 and NO_3^- fluxes were 0.3 to 1.2, −6 to −1, and −1 to 0, respectively.

The optimized parameter values were obtained by finding the coefficient values that gave the lowest overall model-data misfit for O_2 or NO_3^- fluxes. The minimum sum of squares for the entire database of fluxes was obtained with

$$B_0 = 0.5 \quad m = -3.73 \quad n = -0.17 \tag{22}$$

The rate-depth profile of POC degradation can thus now be calculated from the rain rate using equation (12), where B_0, B_1, and B_2 are defined using equations (22), (14), and (21), respectively. B_2 varies between approximately −3.7 and −2.0 for the range of RRPOC in the database, which is more negative than the exponent −0.95 in the *Middelburg* [1989] model yet more similar to the range of −1.7 to −1.4 derived for shallow subsurface sediments by *Jørgensen and Parkes* [2010]. Values ranging from −2.6 to −2.0 were determined for muddy Holocene sediments in Aarhus Bay by S. Flury et al. (Controls on subsurface methane fluxes and shallow gas formation in Baltic Sea sediment (Aarhus Bay, Denmark), submitted to *Geochimica et Cosmochimica Acta*, 2015).

The measured versus modeled O_2 and NO_3^- fluxes using this function are shown in Figure 3. O_2 fluxes could be simulated at 180 stations (97% of all stations) and mostly within 25% of the measurements. Modeled NO_3^- fluxes were simulated at 132 sites (71% of total). Paired O_2 and NO_3^- fluxes were simulated at 131 stations within 50% tolerance limits (71% of all stations). Thus, the performance of the transfer function largely depends on its ability to simulate NO_3^- fluxes. The mean relative error of the calculated NO_3^- flux is 48%, which can be broadly assumed to represent the uncertainty in the simulated degradation rate function.

Most outlying NO_3^- data were associated with low nitrate fluxes (<0.5 mmol m^{-2} d^{-1}) on the shelf (<200 m) and upper slope (>200–1000 m) where 60% of sites were fitted. Despite relatively high rates of denitrification, these

sites are characterized by low nitrate fluxes because nitrification at these sites creates a weak NO_3^- concentration gradient at the sediment surface and hence low diffusive flux [e.g., *Devol et al.*, 1997; *Berelson et al.*, 1998]. A large error for simulating low NO_3^- fluxes is to be expected because, as mentioned, small absolute differences in the flux are likely to be associated with a high relative error. Oxygen does not suffer from the same uncertainties because (i) the sediments always act as a sink for O_2 and (ii) the O_2 flux is closely linked to the POC rain rate, whereas NO_3^- flux is not.

The weakness of the model to accurately simulate the low NO_3^- fluxes on the shelf is rooted in the global parameterizations of biologically mediated transport and kinetic processes. To demonstrate this point, NO_3^- fluxes for individual stations lying outside of the tolerance limits could be better simulated by fine tuning the parameterization of bioirrigation rates as well as nitrification (not shown). However, applying the same adjustments to the other fitted stations resulted in a loss of model accuracy for those stations. Thus, it is our opinion that no single set of biogeochemical and transport parameters is able to simulate all the shelf sites simultaneously, such that the number of fitted stations cannot be increased with the empirical transport functions currently used.

We also observed that NO_3^- fluxes at many of the outlying sites could not be fit with the model for a broad range of *m* and *n* coefficients. These include sites on the Peru margin [*Bohlen et al.*, 2011], the Mid-Atlantic Bight [*Laursen and Seitzinger*, 2002], and Monterey Bay [*Berelson et al.*, 2003]. Bottom waters on the Peru margin are near anoxic, and here the model underestimated the NO_3^- flux into the sediment. We suspect that biological NO_3^- transport by vacuolated bacteria (e.g., *Thioploca* spp.) and protists (e.g., foraminifera) enhances NO_3^- uptake at these sites [*Bohlen et al.*, 2011; *Prokopenko et al.*, 2011]. In contrast, the Mid-Atlantic Bight sites are shallow (maximum water depth 15 m) and sandy. The permeability of sand is greater than fine-grained mud, such that boundary layer current and topography interactions will enhance the exchange of pore water with seawater by pressure-driven advective processes [*Huettel et al.*, 1996]. N cycling in sands can thus exhibit large differences compared to fine-grained muds [e.g., *Cook et al.*, 2006; *Rao et al.*, 2007]. N fluxes in shallow sediments also tend to display high seasonal variability, as exemplified in the Monterey Bay data. More generally, it is likely that intraannual variability and sediment grain size effects play an important role in generating the observed misfit between modeled and measured NO_3^- fluxes on the continental shelf.

4.2. Further Model Ground Truthing

The predictive function relating carbon reactivity with rain rate is primarily constrained by the large database of O_2 and NO_3^- fluxes. As further validation of the approach, model results were compared with sediment geochemical data as well as global rates of POC burial and denitrification.

4.2.1. Sediment Profiles

Measured O_2 and NO_3^- profiles are mostly unavailable at the sites in our database. Therefore, we selected sites where pore water data were available from key ocean settings including the continental shelf (41 and 114 m), slope (241 and 1025 m), and deep sea (3073 m) (Figure 4). Two of these sites, stations WE206 and 241 on the Washington and Mauritanian margin (respectively), are located in high-nitrate-low-oxygen (HNLO) areas where oxygen-deficient waters impinge on the seafloor. In general, the model captures the trends in NO_3^- and O_2 profiles through the bioturbated layer, although imperfectly. At the deep-sea site in the Southern Ocean (PS2361-1), for example, the model underestimates the increase in NO_3^- concentration below the sediment surface due to nitrification [*Smetacek et al.*, 1997]. The model also predicts that O_2 is not depleted within the upper 10 cm. Although corroborating field data are unavailable here, incomplete O_2 consumption in the bioturbated layer in deep-sea sediments is to be expected due to very low rates of carbon degradation [*Wenzhöfer and Glud*, 2002]. Bioirrigation is responsible for the small subsurface peak in modeled NO_3^- at St. NH14A on the Washington margin. The same peak is seen at St. 241 on the Mauritanian margin in both the field and modeled data. However, the model tends to underestimate POC content at the same site (Figure 4c). This is very likely due to much higher measured sediment accumulation rates in this productive margin of 0.35 cm yr^{-1} [*Dale et al.*, 2014] compared to the value of 0.05 cm yr^{-1} calculated using the generic algorithm based on water depth [*Burwicz et al.*, 2011]. In

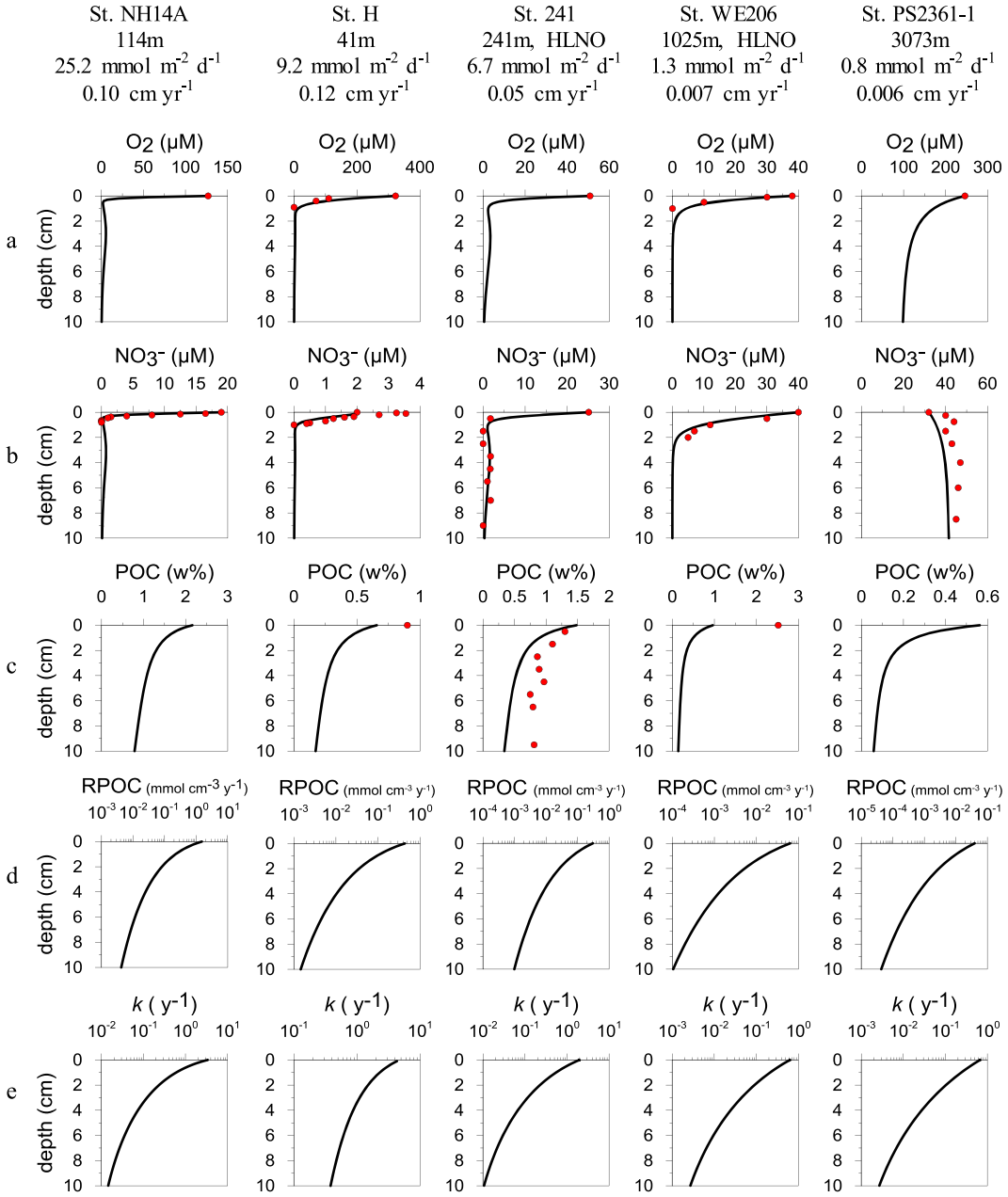

Figure 4. Model-predicted (curves) and measured (red circles) (a) O_2 and (b) NO_3^- concentrations, (c) POC content, (d) POC degradation rate, RPOC, and (e) the first-order mineralization constant, *k*, in the bioturbated layer for several stations. As indicated at the top of the figure, the stations differ in their water depth, POC rain rate (in mmol m^{-2} d^{-1}), and sedimentation rate (in cm yr^{-1}) derived from the water depth (Table 1). References for stations (see Table S1 in the supporting information): St. NH14A = Washington margin [*Devol and Christensen*, 1993], St. H = Arctic shelf [*Devol et al.*, 1997], St. 241 = Mauritanian margin [*Dale et al.*, 2014], St. WE206 = Washington margin [*Hartnett and Devol*, 2003], and St. PS2361-1 = Southern Ocean [Supplement to *Smetacek et al.*, 1997].

general, though, POC contents of up to 2% on the shelf and <0.5% in the deep sea agree well with global data sets [*Seiter et al.*, 2004].

We further compared modeled and measured nitrate penetration depth (NPD) for an additional set of 30 stations that was used to validate the Muds model [*Archer et al.*, 2002]. NPD should be sensitive to our predictive function because RPOC(*x*) determines the depth where organic matter is degraded and thus the

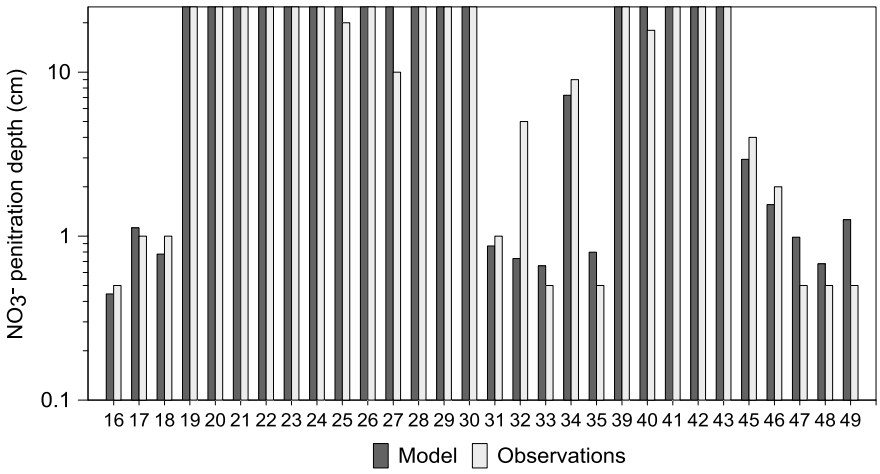

Figure 5. Comparison of measured (blue) and simulated (red) nitrate penetration depths (NPD in cm, log scale) for sites compiled by *Archer et al*. [2002] that are independent to those in our database. The numbering on the *x* axis denotes the data set number given in Table 2 in *Archer et al*. [2002]. For most sites, the NPD exceeded the core length (25 cm); i.e., nitrate was not fully depleted at the base of the core sediment depth. The vertical axis is thus clipped at 25 cm. Modeled NPD agrees with the measurements for all sites except #25, 27, 32, and 40.

depth where NO_3^- is consumed (by denitrification) and produced (by nitrification). NPD was defined as the sediment depth where NO_3^- concentration falls to 2% of the local bottom water level. RRPOC and bottom water O_2 and NO_3^- are available for these stations and were used as boundary conditions. The results demonstrate that the model is able to predict the NPD at 26 out of 30 stations (87%) to within 50% or 1 cm (Figure 5). At many deep-sea stations, the NPD exceeded 25 cm, analogous to the Southern Ocean site in Figure 4e. These results are encouraging because the 30 stations were not included in our original database and so constitute independent validation of our model.

4.2.2. Global POC Burial and Denitrification Rates

Global predictions of POC burial and denitrification were made by applying the benthic model on a gridded ocean seafloor. Spatially resolved bathymetry, bottom water temperature, O_2 and NO_3^- concentrations, and RRPOC data on a $1° \times 1°$ resolution were taken from *Bohlen et al*. [2012]. The model was forced using these boundary conditions for each grid point on the continental margin ($\leq$2000 m) and at a coarser resolution ($10° \times 10°$) for the deep sea ($>$2000 m). Sedimentation rates and mixing by bioturbation were calculated as previously, whereas bioirrigation was determined assuming that RRPOC is a good approximation for sediment oxygen uptake (see Table 2).

Benthic denitrification rates were calculated as the sum of canonical denitrification and anammox at each grid point. Integrating globally gives a total N loss of $182 \pm 88\,\mathrm{Tg\,yr^{-1}}$ of N, where the error denotes model uncertainty (48%) discussed above (Table 3). This agrees well with other predictions based on diverse approaches including mass balances, benthic models, and ESMs (93–2030 $\mathrm{Tg\,yr^{-1}}$). Global POC burial rates calculated at the base of the bioturbation zone amount to $107 \pm 52\,\mathrm{Tg\,yr^{-1}}$ of C, which are at the lower end of previous values based on sediment data (Table 3). However, the $1° \times 1°$ grid applied for our estimates does not fully resolve shelf bathymetry and the shelf area is underestimated. The shelf area (0–200 m) is equal to $11.42 \cdot 10^6\,\mathrm{km^2}$ in our grid, whereas high-resolution data predict an area of $27.12 \cdot 10^6\,\mathrm{km^2}$ [*Eakins and Sharman*, 2012]. Furthermore, POC burial fluxes derived from marine productivity and particle export data tend to be much higher than those derived directly using sediment data, possibly because they do not properly consider sediment resuspension on the continental margin and downslope transport [*Burdige*, 2007; *Dunne et al*., 2007]. Our globally averaged CBE of 6.1% is similar to the range of 7.9 to 9.4% reported by *Burdige* [2007] yet markedly lower than determined by ESMs (13–34% [*Dunne et al*., 2007; *Palastanga et al*., 2011]). Bearing in mind that our model was not tuned to POC burial and denitrification rates, the good agreement between our model and previously published rates suggests that the carbon degradation function is suitable for predicting benthic carbon mineralization in global models.

Table 3. Global Rates of POC Burial (Tg yr^{-1} of C) and Benthic Denitrification (Tg yr^{-1} of N) Listed From Highest to Lowest

Rate	Method	Reference
POC burial[a]		
780 (34%)	Earth system model	*Dunne et al.* [2007]
309–637 (7.9–9.4)[b]	Data compilation	*Burdige* [2007]
160	Revised from *Berner* [1982]	*Hedges and Keil* [1995]
140	Data analysis	*Baturin* [2007]
130	Global benthic model	*Wallmann et al.* [2012]
126	Fluvial inputs and burial	*Berner* [1982]
107 ± 52 (6.1 ± 3%)	Global benthic model	This study
30 (13%)	Earth system model	*Palastanga et al.* [2011]
Denitrification		
2030	Global benthic model	*Archer et al.* [2002]
300	Water column data	*Codispoti et al.* [2001]
285	Predictive algorithm	*Middelburg et al.* [1996]
280	Isotope mass balance	*Brandes and Devol* [2002]
190	Box model	*Deutsch et al.* [2004]
182 ± 88	Global benthic model	This study
180	Revised from *Brandes and Devol* [2002]	*Gruber et al.* [2004]
153	Predictive algorithm	*Bohlen et al.* [2012]
149	Earth system model	*Somes et al.* [2013]
146	Global benthic model	*Thullner et al.* [2009]
109	Earth system model	*DeVries et al.* [2013]
93	Box model	*Eugster and Gruber* [2012]

[a]Number in parentheses is the global mean carbon burial efficiency (%) where available.
[b]From a number of independent studies. The range of values considers low POC burial in sandy shelf sediments.

4.2.3. Comparison With Previous Empirical Approaches

Our derived function is conceptually simple and requires only one independent variable (rain rate) to fully describe the depth distribution of the rate of carbon degradation in the bioturbated zone. From a practical standpoint, it is desirable to be able to describe benthic POC degradation in ESMs using a master variable that is well known at the global scale. This avoids the use of parameterizations based on site-specific data and allows for more realistic nonsteady state model experiments as well as future and paleo-applications. Alternative empirical relations for the apparent rate constant of aerobic (k_{aer}) and anaerobic (k_{anaer}) organic matter mineralization versus sedimentation rate have been widely cited [*Müller and Mangini*, 1980; *Toth and Lerman*, 1977; *Tromp et al.*, 1995]:

$$k_{aer} = 2.97\,\omega_{acc}^{\ 0.62} \tag{23a}$$

$$k_{anaer} = 0.057\,\omega_{acc}^{\ 1.94} \tag{23b}$$

These relations show that for a given sedimentation rate, the rate constant decreases by 2 to 3 orders of magnitude from the oxidized surface to the underlying anoxic layers. This huge disparity may reflect the fact that a fraction of fresh labile material is extremely reactive and already respired aerobically by the time it reaches the anaerobic sediment layers, rather than being specific to electron acceptors [*Ingall and Van Cappellen*, 1990; *Middelburg et al.*, 1993]. Furthermore, the sharp discontinuity between the rate constants for aerobic and anaerobic mineralization is contrary to the continuum nature of the reactivity of marine organic matter [*Middelburg*, 1989; *Boudreau and Ruddick*, 1991].

Focusing on the bulk carbon pool mineralized in the bioturbated layer (upper 10–20 cm), *Boudreau* [1997] compiled data from various sites worldwide ($n = 23$) and also proposed a relationship between sedimentation rate and the rate constant, which he termed k_1:

$$k_1 = 0.38 \cdot \omega_{acc}^{\ 0.59} \tag{24}$$

k_1 can be assumed to represent the mean reactivity of the organic matter mineralized in the specified layer, although the highly reactive fractions mineralized on daily/weekly time scales are not captured by this function [*Boudreau*, 1997].

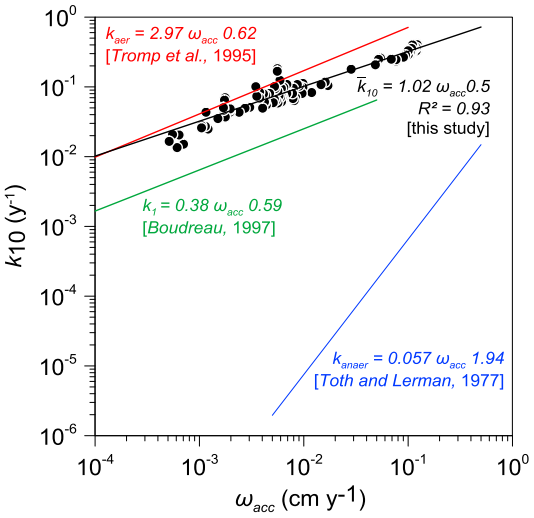

Figure 6. Relationship between the mean first-order rate constants ($\overline{k}$) in the bioturbated layer (upper 10 cm) versus sedimentation rate at the stations from the database (black symbols and regression curve). The green line indicates the function derived by *Boudreau* [1997], and the red and blue lines are the rate constants for aerobic and anaerobic organic matter mineralization proposed by *Tromp et al.* [1995] and *Toth and Lerman* [1977], respectively. Note that these previous functions are all empirically derived and the data are omitted here for clarity.

We compared our model results with these empirical relationships by first calculating the apparent depth-dependent first-order rate constant for POC degradation, k (year^{-1}). This was achieved by dividing the simulated RPOC(x) by the simulated POC content (in consistent units):

$$k(x) = \frac{\mathrm{RPOC}(x)}{\mathrm{POC}(x)} \tag{25}$$

As an example, depth profiles of RPOC(x), POC content, and $k(x)$ are calculated for the stations in Figure 4. The first-order rate constant $k(x)$ decreases rapidly with sediment depth by several orders of magnitude over the bioturbated zone (Figure 4e). This reflects the increasingly refractive nature of POC below the sediment surface and implies that most POC (75%, data not shown) will be degraded in the uppermost 1–2 cm, in accordance with observations [*Hedges et al.*, 1999]. Note that this is true even for the deep-sea site where simulated O_2 is not depleted over the upper 10 cm. This further agrees with calculations of *e*-folding depths for organic matter decomposition of 0.3 to 3 cm in pelagic sediments [*Martin and Sayles*, 1996]. These workers showed that highly reactive fractions accounted for over 60% of bulk POC mineralization at two thirds of the sites investigated. Calculated $k(x)$ values at the sediment surface also vary with water depth, decreasing from 4 to 5 yr^{-1} on the shelf to 0.75 yr^{-1} in the deep sea due to mineralization of reactive organic matter during transit through the water column [e.g., *Martin et al.*, 1987].

The mean k over a defined sediment depth, $\overline{k}_x$, can then be calculated as

$$\overline{k}_x = \frac{1}{x}\int_0^x k(x)\mathrm{d}x \tag{26}$$

The mean k for the bioturbated layer (upper 10 cm) for all the fitted stations in the database was described by the following power law (Figure 6):

$$\overline{k}_{10} = 1.02 \cdot \omega_{\mathrm{acc}}{}^{0.5} \tag{27}$$

For the stations in the database, $\overline{k}_{10}$ ranges from 0.01 to 0.4 year^{-1}. The scaling coefficient in equation (27) is higher than predicted by Boudreau's function (1.02 versus 0.38), which probably derives from very high POC mineralization rates close to the sediment-water interface which were not considered in his function for k_1. It is interesting to note that our $\overline{k}_{10}$ values are much closer to the empirical function for aerobic mineralization compared to anaerobic mineralization (equations (23a) and (23b)). This shows that the mean rate of organic matter degradation in the bioturbated zone is dominated by the very reactive fractions degraded in the oxidized layer, even though bioturbated sediments deposited at continental margins quickly become anoxic within a few millimeters [*Wenzhöfer and Glud*, 2002]. Importantly, however, the rapid decrease in k with sediment depth (Figure 4e) clearly illustrates that the use of a 1-G model is conceptually incorrect.

4.3. Implications for Global Rates of Benthic O_2 and NO_3^- Uptake

Global model applications that explicitly consider benthic POC degradation in a 1-D framework typically do not calculate RPOC(x) a priori. Instead, RPOC(x) is calculated directly from POC content and a predefined first-order rate constant(s), in other words, a G-type model. For example, the HAMOCC2 ESM uses a pseudo-2-G model, whereby one POC pool is simulated with different prescribed rate constants for aerobic and

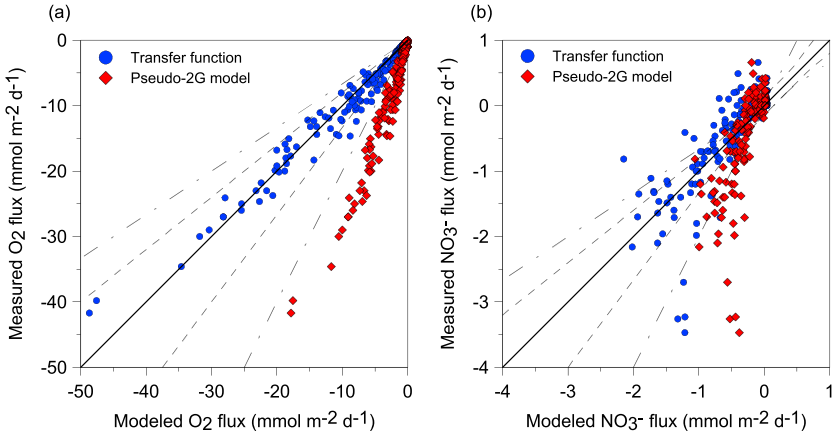

Figure 7. Comparison of measured versus modeled benthic fluxes of (a) O_2 and (b) NO_3^- using the optimized parameters of the transfer function (equation (21)) and first-order kinetic constants in the pseudo-2-G model from *Palastanga et al.* [2011]. The solid line indicates 1:1 line (measured = modeled), the dashed lines indicate the 25% deviation, and the dash-dotted lines indicate the 50% deviation.

anaerobic respiration [*Palastanga et al.*, 2011]. The DCESS model takes a similar approach, although in that case the rate constants depend on bioturbation intensity and rain rate [*Shaffer et al.*, 2008]. The diagenetic "Muds" model parameterizes *k* for discrete carbon respiration pathways as a function of the bioturbation coefficient or rain rate [*Archer et al.*, 2002]. Vertically integrated benthic models have also been used to calculate POC degradation rates using a single rate constant, as commonly employed by the Baltic Sea modeling community [*Neumann et al.*, 2002; *Eilola et al.*, 2009; *Gustafsson*, 2012]. In those cases, the rate constants are often tuned to tracer distributions in the water column rather than benthic flux or geochemical data. Other examples abound in the literature (reviewed by *Arndt et al.* [2013]), which attests to the current lack of consensus of how best to parameterize benthic POC mineralization.

We calculated global POC burial and denitrification rates with our model by adopting the pseudo-2-G approach used in HAMOCC2 as an example of other published approaches [*Palastanga et al.*, 2011]. Reaction and transport rates were calculated as previously after modifying the POC degradation rate to be the product of POC content and the first-order rate constants used by *Palastanga et al.* [2011]. The constants were defined according to aerobic (k_{ox}) and anaerobic POC respiration (k_{ax}). k_{ox} was equal to 0.01 $year^{-1}$ for water depths $<$2000 m and 0.005 $year^{-1}$ for depths $>$2000 m, whereas k_{ax} values were lower in both regions (0.008 and 0.002 $year^{-1}$, respectively). These rate constants were tuned to surface POC content measurements in HAMOCC2, although the prime focus of the study was long-term (10–100 kyr) P and O_2 dynamics in the ocean [*Palastanga et al.*, 2011].

O_2 fluxes calculated using the pseudo-2-G model are significantly underestimated by around a factor of 3 compared to the database (Figure 7). NO_3^- fluxes are approximately half the measured values. In view of the fact that ODU loss from the sediment is minimal, these findings imply that the bulk reactivity of POC using the prescribed rate constants is too low and that insufficient water column O_2 is respired by the sediments. Consequently, too little POC is degraded. Global POC burial rates estimated by upscaling the model using the gridded data as before indeed show that POC burial equals 840 Tg yr^{-1} compared to 107 Tg yr^{-1} using the transfer function (Table 3), which is equivalent to a global CBE of 48%. Interestingly, the global denitrification rate (177 Tg N y^{-1}) is very similar to the previous value of 182 Tg N y^{-1} despite the offset in NO_3^- fluxes (Figure 7b). We believe this to be coincidental, resulting from a greater importance of coupled nitrification-denitrification compensating for reduced rates of denitrification fueled by NO_3^- diffusing into the sediment from the overlying water column.

This exercise does not invalidate the results of *Palastanga et al.* [2011] since the physical and biogeochemical structures of their diagenetic model are very different to ours. Furthermore, the global distribution of bottom water redox conditions and POC rain rate in HAMOCC2 may differ from the the gridded maps used here. It shows, however, that surface POC content may not be the ideal metric to validate benthic models where fluxes of redox-sensitive species are the research focus. More importantly, it highlights the lack of a

generalized and transferable approach for incorporating benthic processes in ESMs at the regional and global scales [*Arndt et al*., 2013]. Proper consideration of this aspect is critical to determine the benthic feedbacks on the coupled carbon-climate system on time scales similar to the oceanic N and P residence times (10^3–10^4 year). This includes seafloor buffering of CO_2 due to carbonate dissolution. At present, the global rate of carbonate dissolution in sediments due to metabolically derived CO_2, that is, originating from organic matter respiration, is very poorly constrained. We propose that our parameterization of POC mineralization would greatly improve our understanding of these feedbacks in ESMs.

5. Conclusions

Marine sediments regulate the long-term balance of oceanic nutrients and atmospheric O_2. Yet there is no consensus of how benthic mineralization should be parameterized in Earth system models (ESM) that couple climate dynamics with marine and terrestrial biogeochemistry. In this study, a straightforward function to calculate the depth-dependent rate of POC degradation in bioturbated marine sediments at the global scale was derived by simulating O_2 and NO_3^- fluxes at 185 stations using a diagenetic model. The rate was described using a power function characterized by three empirical coefficients, one of which (B_0) has a fixed value and the other (B_1) is obtainable from the third (B_2) and the POC rain rate to the seafloor. The simplicity of this function allows carbon degradation rates in surface sediments to be constrained from one governing variable that is routinely used in ESMs, i.e., POC rain rate. It also captures the essential elements of the continuum nature of organic matter degradation in sediments as opposed to the parameter-intensive multi-G approach. Using this function, O_2 and NO_3^- fluxes were simulated at 71% of all stations. Although by no means a perfect agreement, the function does predict global denitrification and POC burial rates that are well within previous estimates. The function is not suitable to simulate NO_3^- fluxes in sandy sediments, which may contribute to the uncertainty in global POC burial and denitrification rates. Very low NO_3^- fluxes on the shelf and slope are also not captured due the complex and heterogeneous environmental conditions encountered there. This alludes to a more general problem of predicting benthic fluxes on the shelf and suggests that no single model is suitable for these environments. Nonetheless, the function provides a basis for more accurately simulating POC degradation considering the downcore decrease in POC reactivity in the bioturbated zone.

The distribution of POC degradation rates in surface sediments has a fundamental effect on key benthic processes. Our model predicts that most of the POC degradation occurs within the top sediment layer. Therefore, metabolites produced via POC degradation, such as dissolved phosphorus and CO_2, can largely escape into the overlying bottom water. Only a minor fraction may be consumed by secondary reactions, e.g., the dissolution of pelagic carbonate by metabolic CO_2 and the precipitation of authigenic phosphorus minerals. Conventional 1-G models tend to overestimate rates of secondary reactions since a larger portion of the total POC degradation is allocated in deeper sediment horizons where the metabolites accumulate, precipitate, or react with sediment components. ESMs aiming to simulate benthic POC degradation, pelagic carbonate dissolution, and N and P turnover in sediments could thus be enhanced by coupling the ocean model to the simple benthic module presented in this paper.

Acknowledgments
The empirical data used in this paper are available in the published scientific papers listed in the supporting information. This work is a contribution of the Sonderforschungsbereich 754 "Climate-Biogeochemistry Interactions in the Tropical Ocean" (www.sfb754.de) financially supported by the Deutsche Forschungsgemeinschaft (DFG). We are indebted to Ivan L'Heureux (University of Ottawa) for his discussions and advice on our work. Constructive comments by David Burdige and one anonymous reviewer were very much appreciated.

References

Alonso-Pérez, F., and C. G. Castro (2014), Benthic oxygen and nutrient fluxes in a coastal upwelling system (Ria de Vigo, NW Iberian Peninsula): Seasonal trends and regulating factors, *Mar. Ecol. Prog. Ser.*, *511*, 17–32.

Anderson, L. A. (1995), On the hydrogen and oxygen content of marine phytoplankton, *Deep Sea Res., Part I*, *42*, 1675–1680.

Archer, D. E., J. L. Morford, and S. R. Emerson (2002), A model of suboxic sedimentary diagenesis suitable for automatic tuning and gridded global domains, *Global Biogeochem. Cycles*, *16*(1), 1017, doi:10.1029/2000GB001288.

Arndt, S., B. B. Jørgensen, D. E. LaRowe, J. J. Middelburg, R. D. Pancost, and P. Regnier (2013), Quantifying the degradation of organic matter in marine sediments: A review and synthesis, *Earth Sci. Rev.*, *123*, 53–86.

Baturin, G. N. (2007), Issue of the relationship between primary productivity of organic carbon in ocean and phosphate accumulation (Holocene–Late Jurassic), *Lithol. Miner. Resour.*, *42*, 318–348.

Berelson, W. M., D. Heggie, A. Longmore, T. Kilgore, G. Nicholson, and G. Skyring (1998), Benthic nutrient recycling in Port Phillip Bay, Australia, *Estuarine Coastal Shelf Sci.*, *46*, 917–934.

Berelson, W. M., J. McManus, K. Coale, K. Johnson, D. Burdige, T. Kilgore, D. Colodner, F. Chavez, R. Kudela, and J. Boucher (2003), A time series of benthic flux measurements from Monterey Bay, Calif., *Cont. Shelf Res.*, *23*, 457–481.

Berelson, W., J. McManus, S. Severmann, and C. Reimers (2013), Benthic flux of oxygen and nutrients across Oregon/California shelf sediments, *Cont. Shelf Res.*, *55*, 66–75.

Berg, P., S. Rysgaard, and B. Thamdrup (2003), Dynamic modeling of early diagenesis and nutrient cycling, A case study in an Arctic marine sediment, *Am. J. Sci.*, *303*, 905–955.
Berner, R. A. (1980), *Early Diagenesis—A Theoretical Approach*, Princeton Univ. Press, Princeton, N. J.
Berner, R. A. (1982), Burial of organic carbon and pyrite sulfur in the modern ocean: Its geochemical and environmental significance, *Am. J. Sci.*, *282*, 451–473.
Bohlen, L., A. W. Dale, S. Sommer, T. Mosch, C. Hensen, A. Noffke, F. Scholz, and K. Wallmann (2011), Benthic nitrogen cycling traversing the Peruvian oxygen minimum zone, *Geochim. Cosmochim. Acta*, *75*, 6094–6111.
Bohlen, L., A. W. Dale, and K. Wallmann (2012), Simple transfer functions for calculating benthic fixed nitrogen losses and C:N:P regeneration ratios in global biogeochemical models, *Global Biogeochem. Cycles*, *26*, GB3029, doi:10.1029/2011GB004198.
Boudreau, B. P. (1996), A method-of-lines code for carbon and nutrient diagenesis in aquatic sediments, *Comput. Geosci.*, *22*, 479–496.
Boudreau, B. P. (1997), *Diagenetic Models and Their Implementation*, 414 pp., Springer, Berlin.
Boudreau, B. P., and R. H. Bennett (1999), New rheological and porosity equations for steady-state compaction, *Am. J. Sci.*, *299*, 517–528.
Boudreau, B. P., and B. R. Ruddick (1991), On a reactive continuum representation of organic matter diagenesis, *Am. J. Sci.*, *291*, 507–538.
Boudreau, B. P., C. Arnosti, B. B. Jorgensen, and D. E. Canfield (2008), Comment on "Physical model for the decay and preservation of marine organic carbon", *Science*, *319*, 1616–1617.
Brandes, J. A., and Devol A. H. (2002), A global marine-fixed nitrogen isotopic budget: Implications for Holocene nitrogen cycling, *Global Biogeochem. Cycles*, *16*(4), 1120, doi:10.1029/2001GB001856.
Burdige, D. A. (2007), Preservation of organic matter in marine sediments: Controls, mechanisms, and an imbalance in sediment organic carbon budgets?, *Chem. Rev.*, *107*, 467–485.
Burwicz, E. B., L. H. Rupke, and K. Wallmann (2011), Estimation of the global amount of submarine gas hydrates formed via microbial methane formation based on numerical reaction-transport modeling and a novel parameterization of Holocene sedimentation, *Geochim. Cosmochim. Acta*, *75*, 4562–4576.
Christensen, E. R. (1982), A model for radionuclides in sediments influenced by mixing and compaction, *J. Geophys. Res.*, *87*, 566–572, doi:10.1029/JC087iC01p00566.
Codispoti, L. A., J. A. Brandes, J. P. Chrstensen, A. H. Devol, S. W. A. Naqvi, H. W. Paerl, and T. Yoshinari (2001), The oceanic fixed nitrogen and nitrous oxide budgets: Moving targets as we enter the anthropocene, *Sci. Mar.*, *65*, 85–105.
Cook, P. L. M., F. Wenzhoefer, S. Rysgaard, O. S. Galaktionov, F. J. R. Meysman, B. D. Eyre, J. Cornwell, M. Huettel, and R. N. Glud (2006), Quantification of denitrification in permeable sediments: Insights from a two-dimensional simulation analysis and experimental data, *Limnol. Oceanogr.: Methods*, *4*, 294–307.
Dale, A. W., S. R. Meyers, D. R. Aguilera, S. Arndt, and K. Wallmann (2012), Controls on organic carbon and molybdenum accumulation in Cretaceous marine sediments from the Cenomanian–Turonian interval including Oceanic Anoxic Event 2, *Chem. Geol.*, *324–325*, 28–45.
Dale, A. W., S. Sommer, E. Ryabenko, A. Noffke, L. Bohlen, K. Wallmann, K. Stolpovsky, J. Greinert, and O. Pfannkuche (2014), Benthic nitrogen fluxes and fractionation of nitrate in the Mauritanian oxygen minimum zone (Eastern Tropical North Atlantic), *Geochim. Cosmochim. Acta*, *134*, 234–256.
Deutsch, C., D. M. Sigman, R. C. Thunell, A. N. Meckler, and G. H. Haug (2004), Isotopic constraints on glacial/interglacial changes in the oceanic nitrogen budget, *Global Biogeochem. Cycles*, *18*, GB4012, doi:10.1029/2003GB002189.
Devol, A. H., and J. P. Christensen (1993), Benthic fluxes and nitrogen cycling in sediments of the continental margin of the eastern North Pacific, *J. Mar. Res.*, *51*, 345–372.
Devol, A. H., L. A. Codispoti, and J. P. Christensen (1997), Summer and winter denitrification rates in western Arctic shelf sediments, *Cont. Shelf Res.*, *17*, 1029–1033.
DeVries, T., C. Deutsch, P. A. Rafter, and F. Primeau (2013), Marine denitrification rates determined from a global 3-D inverse model, *Biogeosciences*, *10*, 2481–2496.
Dhakar, S. P., and D. J. Burdige (1996), Coupled, non-linear, steady state model for early diagenetic processes in pelagic sediments, *Am. J. Sci.*, *296*, 296–330.
Dunne, J. P., J. L. Sarmiento, and A. Gnanadesikan (2007), A synthesis of global particle export from the surface ocean and cycling through the ocean interior and on the seafloor, *Global Biogeochem. Cycles*, *21*, GB4006, doi:10.1029/2006GB002907.
Eakins, B. W., and G. F. Sharman (2012), *Hypsographic Curve of Earth's Surface From ETOPO1*, NOAA Nat. Geophys. Data Cent., Boulder, Colo.
Eilola, K., H. E. M. Meier, and E. Almroth (2009), On the dynamics of oxygen, phosphorus and cyanobacteria in the Baltic Sea: A model study, *J. Mar. Syst.*, *75*, 163–184.
Emerson, S., K. Fisher, C. Reimers, and D. Heggie (1985), Organic carbon dynamics and preservation in deep-sea sediments, *Deep Sea Res., Part A*, *32*, 1–21.
Eugster, O., and N. Gruber (2012), A probabilistic estimate of global marine N-fixation and denitrification, *Global Biogeochem. Cycles*, *26*, GB4013, doi:10.1029/2012GB004300.
Glud, R. N. (2008), Oxygen dynamics of marine sediments, *Mar. Biol. Res.*, *4*, 243–289.
Gruber, N., P. Friedlingstein, C. B. Field, R. Valentini, M. Heimann, J. E. Richey, P. Romero-Lankao, D. Schulze, and C.-T. A. Chen (2004), The vulnerability of the carbon cycle in the 21st century: An assessment of carbon-climate-human interactions, in *The Global Carbon Cycle: Integrating Humans, Climate and the Natural World*, edited by C. Field and M. Raupach, pp. 45–76, Island Press, Washington, D. C.
Gustafsson, B. G. (2012), Modeling the combined impact of changing climate and changing nutrient loads on the Baltic Sea environment in an ensemble of transient simulations for 1961–2099, *Clim. Dyn.*, *39*, 2421–2441.
Hartnett, H. E., and A. H. Devol (2003), Role of a strong oxygen-deficient zone in the preservation and degradation of organic matter: A carbon budget for the continental margins of northwest Mexico and Washington State, *Geochim. Cosmochim. Acta*, *67*, 247–264.
Hedges, J. I., F. S. Hu, A. H. Devol, H. E. Hartnett, E. Tsamakis, and R. G. Keil (1999), Sedimentary organic matter preservation: A test for selective degradation under oxic conditions, *Am. J. Sci.*, *299*, 529–555.
Huettel, M., W. Ziebis, and S. Forster (1996), Flow-induced uptake of particulate matter in permeable sediments, *Limnol. Oceanogr.*, *41*, 309–322.
Hulth S., R. C. Aller, D. E. Canfield, T. Dalsgaard, P. Engström, F. Gilbert, K. Sundbäck, and B. Thamdrup (2005), Nitrogen removal in marine environments: Recent findings and future research challenges, *Mar. Chem.*, *94*, 125–145.
Ingall, E. D., and P. Van Cappellen (1990), Relation between sedimentation rate and burial of organic phosphorus and organic carbon in marine sediments, *Geochim. Cosmochim. Acta*, *54*, 373–386.
Jahnke, R. A., and D. B. Jahnke (2004), Calcium carbonate dissolution in deep sea sediments: Reconciling microelectrode, pore water and benthic flux chamber results, *Geochim. Cosmochim. Acta*, *68*, 47–59.
Jørgensen, B. B. (1978), A comparison of methods for the quantification of bacterial sulfate reduction in coastal marine sediments: II. Calculation from mathematical models, *Geomicrobiol. J.*, *1*, 29–47.

Jørgensen, B. B., and R. J. Parkes (2010), Role of sulfate reduction and methane production by organic carbon degradation in eutrophic fjord sediments (Limfjorden, Denmark), *Limnol. Oceanogr.*, *55*, 1338–1352.
Laursen, A. E., and S. P. Seitzinger (2002), The role of denitrification in nitrogen removal and carbon mineralization in Mid-Atlantic Bight sediments, *Cont. Shelf Res.*, *22*, 1397–1416.
Locarnini, R. A., A. V. Mishonov, J. I. Antonov, T. P. Boyer, H. E. Garcia, O. K. Baranova, M. M. Zweng, and D. R. Johnson (2010), World Ocean Atlas 2009 Volume 1: Temperature. S. Levitus, Ed. NOAA Atlas NESDIS 68, 184 pp., U.S. Gov. Print. Off., Washington, D. C.
Martin, W. R., and F. L. Sayles (1996), $CaCO_3$ dissolution in sediments of the Ceara Rise, western equatorial Atlantic, *Geochim. Cosmochim. Acta*, *60*, 243–263.
Martin, W. R., and F. L. Sayles (2004), Organic matter cycling in sediments of the continental margin in the northwest Atlantic Ocean, *Deep Sea Res., Part I*, *51*, 457–489.
Martin, W. R., and F. L. Sayles (2006), Organic matter oxidation in deep-sea sediments: Distribution in the sediment column and implications for calcite dissolution, *Deep Sea Res., Part II*, *53*, 771–792.
Martin, J. H., G. A. Knauer, D. M. Karl, and W. W. Broenkow (1987), VERTEX: Carbon cycling in the northeast Pacific, *Deep Sea Res., Part A*, *34*, 267–285.
Meile, C., and P. Van Cappellen (2003), Global estimates of enhanced solute transport in marine sediments, *Limnol. Oceanogr.*, *48*, 777–786.
Meile, C., and P. Van Cappellen (2005), Particle age distributions and O_2 exposure times: Timescales in bioturbated sediments, *Global Biogeochem. Cycles*, *19*, GB3013, doi:10.1029/2004GB002371.
Meile, C., P. Berg, P. Van Cappellen, and K. Tuncay (2005), Solute-specific pore water irrigation: Implications for chemical cycling in early diagenesis, *J. Mar. Res.*, *64*, 601–621.
Middelburg, J. J. (1989), A simple rate model for organic matter decomposition in marine sediments, *Geochim. Cosmochim. Acta*, *53*, 1577–1581.
Middelburg, J. J., T. Vlug, and F. J. W. A. Van Der Nat (1993), Organic matter mineralization in marine systems, *Global Planet. Change*, *8*, 47–58.
Middelburg, J. J., K. Soetaert, and P. M. J. Herman (1996), Empirical relationships for use in global diagenetic models, *Deep Sea Res., Part I*, *44*, 327–344.
Müller, P. J., and A. Mangini (1980), Organic carbon decomposition rates in sediments of the Pacific manganese nodule belt dated by ^{230}Th and ^{231}Pa, *Earth Planet. Sci. Lett.*, *51*, 94–114.
Murray, J. W., and K. M. Kuivila (1990), Organic matter diagenesis in the northeast Pacific: Transition from aerobic red clay to suboxic hemipelagic sediments, *Deep Sea Res., Part A*, *37*, 59–80.
Neumann, T., Fennel W., and Kremp C. (2002), Experimental simulations with an ecosystem model of the Baltic Sea: A nutrient load reduction experiment, *Global Biogeochem. Cycles 16*(3), 1033, doi:10.1029/2001GB001450.
Otte, S., J. G. Kuenen, L. P. Nielsen, H. W. Paerl, J. Zopfi, H. N. Schulz, A. Teske, B. Strotmann, V. A. Gallardo, and B. B. Jørgensen (1999), Nitrogen, carbon, and sulfur metabolism in natural Thioploca samples, *Appl. Environ. Microbiol.*, *65*, 3148–3157.
Palastanga, V., C. P. Slomp, and C. Heinze (2011), Long-term controls on ocean phosphorus and oxygen in a global biogeochemical model, *Global Biogeochem. Cycles*, *25*, GB3024, doi:10.1029/2010GB003827.
Prokopenko, M. G., D. M. Sigman, W. M. Berelson, D. E. Hammond, B. Barnett, A. Chong, and A. Townsend-Small (2011), Denitrification in anoxic sediments supported by biological nitrate transport, *Geochim. Cosmochim. Acta*, *75*, 7180–7199.
Rao, A. M. F., M. J. McCarthy, W. S. Gardner, and R. A. Jahnke (2007), Respiration and denitrification in permeable continental shelf deposits on the South Atlantic Bight: Rates of carbon and nitrogen cycling from sediment column experiments, *Cont. Shelf Res.*, *27*, 1801–1819.
Redfield, A. C., B. H. Ketchum, and F. A. Richards (1963), The Influence of organisms on the composition of seawater, in *The Sea*, vol. 2, pp. 26–77, Wiley Intersci., New York.
Reimers, C. E., R. A. Jamnke, and D. C. McCorkle (1992), Carbon fluxes and burial rates over the continental slope and rise off central California with implications for the global carbon cycle, *Global Biogeochem. Cycles*, *6*, 199–224, doi:10.1029/92GB00105.
Rothman, D. H., and D. C. Forney (2007), Physical model for the decay and preservation of marine organic carbon, *Science*, *316*, 1325–1328.
Sarmiento, J. L., and N. Gruber (2006), *Ocean Biogeochemical Dynamics*, 526 pp., Princeton Univ. Press, Princeton, N. J.
Seiter, K., C. Hensen, J. Schröter, and M. Zabel (2004), Organic carbon content in surface sediments—Defining regional provinces, *Deep Sea Res., Part I*, *51*, 2001–2026.
Shaffer, G., O. S. Malskær, and J. O. Pepke Pedersen (2008), Presentation, calibration and validation of the low-order, DCESS Earth System Model (Version 1), *Geosci. Model Dev.*, *1*, 17–51.
Smetacek, V., H. J. W. De Baar, U. V. Bathmann, K. Lochte, and M. M. Rutgers Van Der Loef (1997), Ecology and biogeochemistry of the Antarctic circumpolar current during austral spring: A summary of southern ocean JGOFS cruise ANT X/6 of R.V. Polarstern, *Deep Sea Res., Part II*, *44*, 1–21.
Smith, C. R., R. H. Pope, D. J. DeMaster, and L. Magaard (1993), Age-dependent mixing of deep-sea sediments, *Geochim. Cosmochim. Acta*, *57*, 1473–1488.
Soetaert, K., P. M. J. Herman, and J. J. Middelburg (1996), A model of early diagenetic processes from the shelf to abyssal depths, *Geochim. Cosmochim. Acta*, *60*, 1019–1040.
Somes, C. J., A. Oschlies, and A. Schmittner (2013), Isotopic constraints on the pre-industrial oceanic nitrogen budget, *Biogeosciences*, *10*, 5889–5910.
Teal, L. R., M. T. Bulling, E. R. Parker, and M. Solan (2008), Global patterns of bioturbation intensity and mixed depth of marine soft sediments, *Aquat. Biol.*, *2*, 207–218.
Thullner, M., A. W. Dale, and P. Regnier (2009), Global-scale quantification of mineralization pathways in marine sediments: A reaction-transport modeling approach, *Geochem. Geophys. Geosyst.*, *10*, Q10012, doi:10.1029/2009GC002484.
Toth, D. J., and A. Lerman (1977), Organic matter reactivity and sedimentation rates in the ocean, *Am. J. Sci.*, *277*, 465–485.
Tromp, T. K., P. Van Cappellen, and R. M. Key (1995), A global model for the early diagenesis of organic carbon and organic phosphorus in marine sediments, *Geochim. Cosmochim. Acta*, *59*, 1259–1284.
Van Cappellen, P. (2003), Biomineralization and global biogeochemical cycles, *Rev. Mineral. Geochem.*, *54*, 357–381.
Van Cappellen, P., and Y. Wang (1995), Metal cycling in surface sediments: Modeling the interplay of transport and reaction, in *Metal Contaminated Aquatic Sediments*, edited by H. E. Allen, pp. 64–21, Ann Arbor Press, Chelsea, Mich.
Wallmann, K., E. Pinero, E. Burwicz, M. Haeckel, C. Hensen, A. W. Dale, and L. Ruepke (2012), The global inventory of methane hydrate in marine sediments: A theoretical approach, *Energies*, *5*, 2449–2498.
Wenzhöfer, F., and R. N. Glud (2002), Benthic carbon mineralization in the Atlantic: A synthesis based on in situ data from the last decade, *Deep Sea Res., Part I*, *49*, 1255–1279.

Erratum

In the originally published version of this article, several instances of text contain errors. The following have since been corrected and this version may be considered the authoritative version of record.

In section 3.1, equation 1, "$-(1-\phi(x))\cdot \mathrm{RPOC}(x)$" was changed to "$\frac{\mathrm{RPOC}(x)}{\rho}\cdot\frac{\mathrm{AWC}}{1000}\cdot 100\%$"

In section 3.1, "and RPOC is the rate of POC degradation" was changed to "RPOC is the rate of POC degradation (mmol cm^{-3} yr^{-1} of bulk sediment), AWC (12 g mol^{-1}) is the carbon atomic weight, ρ (2.5 g cm^3) is the dry sediment density and 1000 (mmol mol^{-1}) is a unit conversion factor."

In section 3.1, equation 3, "$\phi(f) - (\phi(0)$" was changed to "$\phi(f) + (\phi(0)$"

In section 3.1, Table 1, the Rate Expression column, "RPOC" was changed to "$\frac{\mathrm{RPOC}}{\phi(x)}$"

In section 3.1, Table 1, footnote a, the following text was added: R_1 to R_4 correspond to carbon degradation, and the rates of production and consumption of other species follow the stoichiometry indicated.

In section 3.3 before equation 12, "(mmol cm^{-3} yr^{-1})" was changed to "(mmol cm^{-3} yr^{-1} of bulk sediment)"

In section 3.3, equation 14, "$(B_2 - 1)$" was changed to "$-(1 + B_2)$"

In Figure 4, the POC and k plots were modified.